Supporting Information

J-Type Hetero-Exciton Coupling Effect on an Asymmetric Donor–Acceptor–Donor-Type Fluorophore

Yuichi Kitagawa[†*], *Ryuto Yachi*[‡], *Takayuki Nakanishi*[†], *Koji Fushimi*[†], *and Yasuchika Hasegawa*[†*]

[†]Faculty of Engineering, Hokkaido University, Kita-13 Jo, Nishi-8 Chome, Kita-ku, Sapporo, Hokkaido, 060-8628, Japan. [‡]Graduate School of Chemical Sciences and Engineering, Hokkaido University, Kita-13 Jo, Nishi-8 Chome, Kita-ku, Sapporo, Hokkaido, 060-8628, Japan.

Corresponding Author

*E-mail: y-kitagawa@eng.hokudai.ac.jp

*E-mail: hasegaway@eng.hokudai.ac.jp

S1. Synthetic schemes

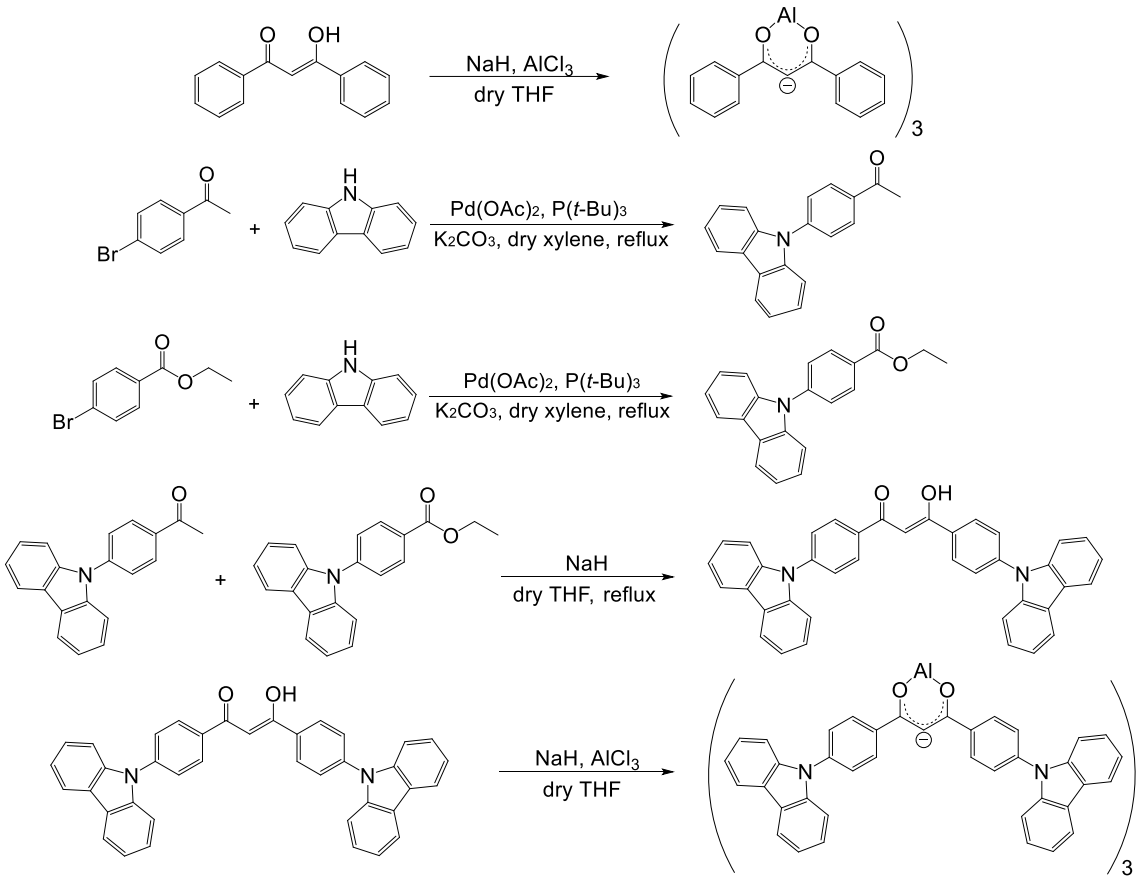

Scheme S1. Synthetic schemes.

S2. Synthetic schemes and their identifications

Carbazole (D)

^{1}H-NMR (400 MHz, DMSO-d_6, TMS): δ/ppm = 7.14-7.25 (2H, m), 7.37-7.48 (2H, m), 7.49-7.57 (2H, m), 8.15 (2H, d, *J* = 8.0 Hz), 11.3 (1H, s).

Dibenzoylmethane (A)

^{1}H-NMR (400 MHz, $CDCl_3$, TMS): δ/ppm = 6.87 (1H, s), 7.45-7.61 (6H, m), 7.96-8.04 (4H, m), 16.9 (1H, s).

Tris(1,3-diphenyl-1,3-propanedionato)aluminium (III) (Al(III)A_3)

The Al(III)A_3 was prepared according to previously reported procedures. A solution of THF, Super Dehydrated (70 mL) was added dropwise to a three-necked flask containing A (0.672 g, 3.00 mmol), Al(III)Cl_3 (0.142 g, 1.05 mmol), NaH (0.147 g, 3.37 mmol), and subsequently stirred for 24 h at room temperature. The product was extracted with CH_2Cl_2, and the extracts were washed three times with distilled water and subsequently dried over anhydrous $MgSO_4$. The solvent was reprecipitated (hexane/CH_2Cl_2), which results in a white solid compound.

^{1}H-NMR (400 MHz, $CDCl_3$, TMS): δ/ppm = 6.95 (3H, s), 7.33-7.51 (18H, m), 7.98-8.09 (12H, m).

S3. ^{1}H-NMR spectrum of As–D–A–D in CD_2Cl_2

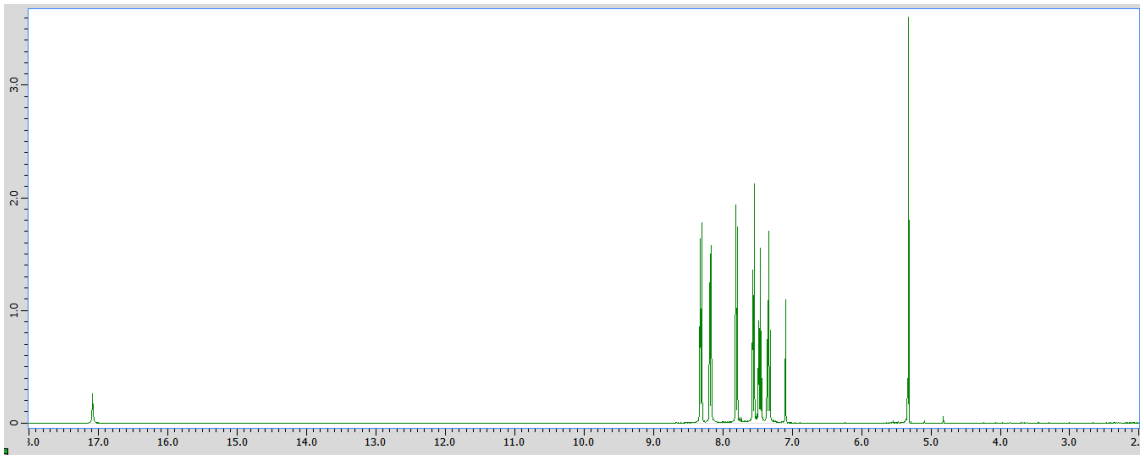

Figure S1. ^{1}H-NMR spectrum for As–D–A–D in CD_2Cl_2.

S4. DFT calculations for As–D–A–D

The optimized structures (Figure S2) of keto and cis-enol forms were calculated by DFT (B3LYP/6-31G(D)). The total electron energy of the cis-enol form was lower than that of the keto form (ΔE = 302 cm^{-1}).

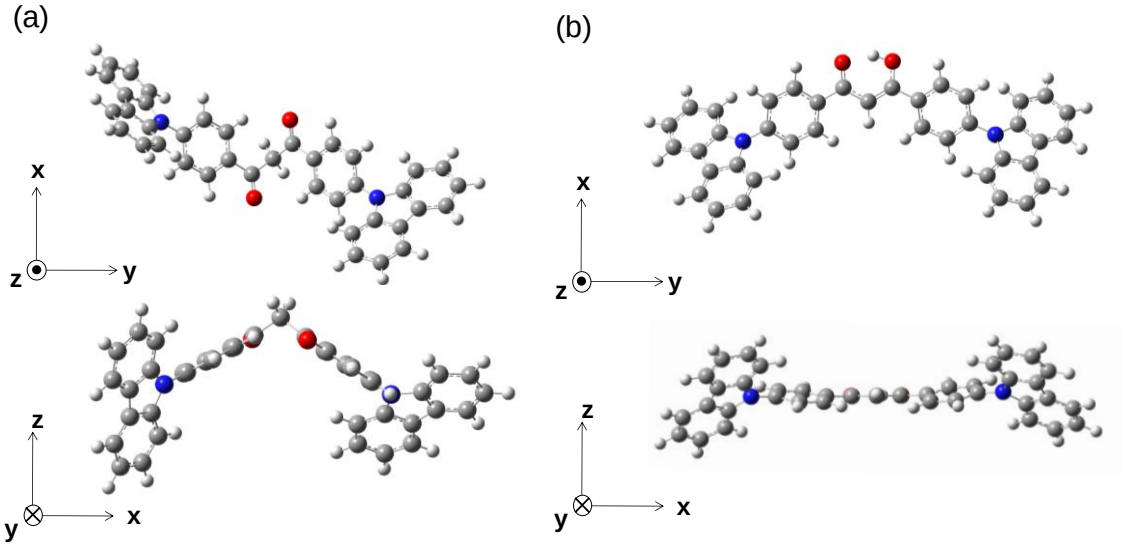

Figure S2. Optimized structures for the keto-form (a) and cis-enol-form (b).

S5. Electronic absorption spectra of A and Al(III)A_3

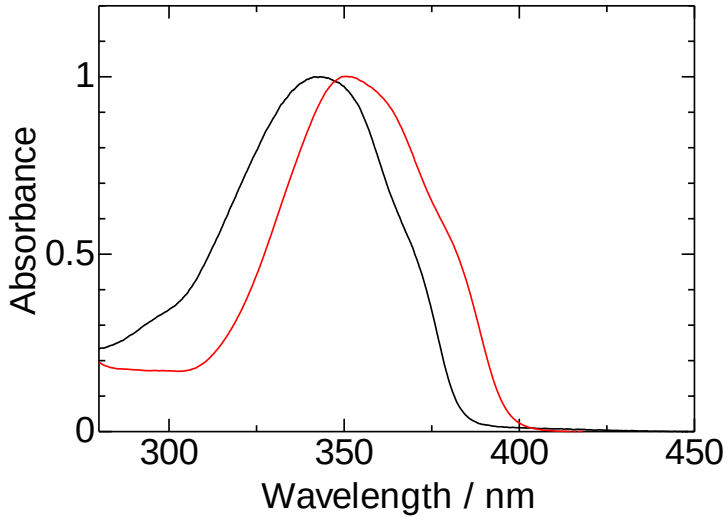

Figure S3. Electronic absorption spectra of A (black line) and Al(III)A_3 (red line).

S6. DFT calculation for As–D–A–D in ground states

In order to clarify the ground state properties, TD-DFT calculations were performed. First, the optimum structure of As–D–A–D in its ground state was calculated by the DFT method (B3LYP/6-31G*, Gaussian03). The optimum structure of As–D–A–D showed a low twisted angle (50.35º and 50.85º) between D and A moieties (Figure S2b). The molecular orbitals are shown in Figure S4. The low twist induces weak delocalization of the orbital between D and A moieties (HOMO and HOMO-1). An electronic absorption spectrum was calculated for the optimum structure of As–D–A–D using the TD-DFT (B3LYP/6-31G*, Gaussian 03) method, and the obtained results can explain the experimental results (Table S1). The three characteristic intense absorption bands were calculated. The intense band at the longest wavelength side was originated from a HOMO →LUMO electronic configuration. The transition from the delocalized orbital between D and A moieties (HOMO) to the localized A orbital (LUMO) caused the observed broad absorption band with a weak CT character. This transition feature indicated that the exciton coupling between the excited states corresponding to the transitions from each donor to acceptor does not take place in the ground-state structure. The calculated second intense absorption band originated from HOMO-4→LUMO electronic configuration, which was assigned to the localized excited states of the As–D–A–D moiety. The experimental broad bands of As–D–A–D and Sy–D–A–D were mainly composed of these transitions. The sharp intense bands of the compounds at around 290 nm mainly originated from HOMO-3→LUMO+2 and HOMO-2→LUMO+3, which were assigned to the localized excited states of the D moiety. In addition, the electronic absorption change behavior upon coordination of Al^{3+} originated from the low electronegativity effect of Al^{3+}, which is expected to induce an increase in the energy of the orbitals with

regard to the transition for the A moiety.

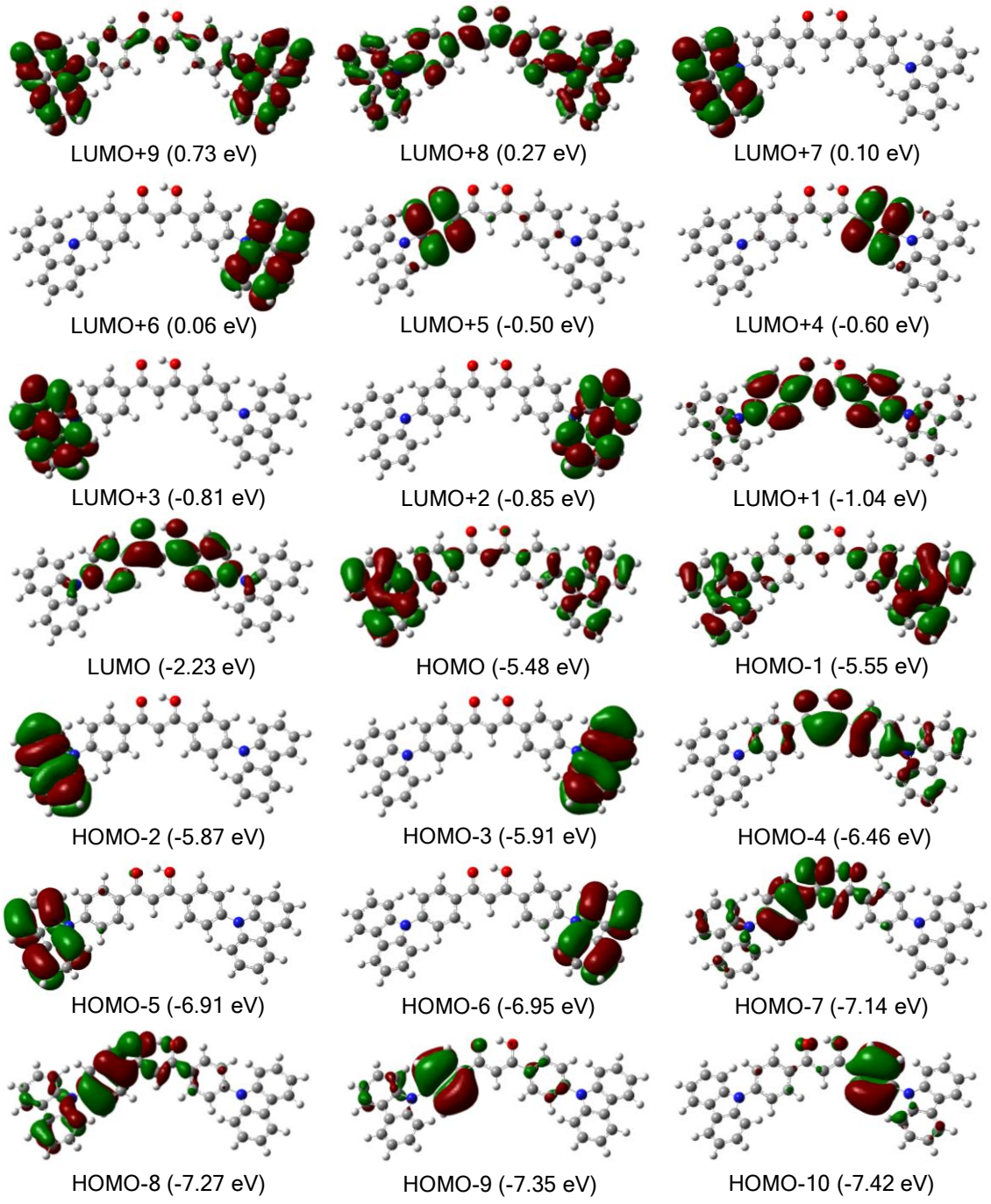

Figure S4. MOs for As–D–A–D in the ground state structure.

Table S1. Information about the main electronic configurations for As–D–A–D.

Excited states	λ_{em} / nm	f_{osc} / -	Main configurations
S_1	437	0.5788	H→L (96 %)
S_2	417	0.0603	H-1→L (97 %)
S_3	379	0.0001	H-2→L (99 %)
S_4	376	0.0001	H-3→L (99 %)
S_5	333	0.0013	H-7→L (68 %), H-8→L (26 %)
S_6	321	0.7345	H-4→L (87 %), H→L+1 (5 %)
S_7	308	0.0455	H-4→L (5 %), H→L+1 (87 %)
S_8	306	0.0075	H-3→L+5 (5 %), H-1→L+2 (59 %), H→L+2 (27 %)
S_9	306	0.0163	H-2→L+6 (5 %), H-1→L+3 (18 %), H→L+3 (67%)
S_{10}	304	0.0208	H-1→L+2 (89 %)
S_{11}	293	0.0058	H-10→L (8 %), H-1→L+4 (54 %), H→L+4 (28%)
S_{12}	291	0.0004	H-9→L (9 %), H-5→L (30 %), H-1→L+5 (9%), H→L+5 (42%)
S_{13}	287	0.0008	H-5→L (65 %), H-1→L+5 (5 %), H-7→L (22 %)
S_{14}	286	0.0013	H-6→L (93 %)
S_{15}	281	0.0001	H-2→L+1 (95 %)
S_{16}	278	0.0001	H-1→L+2 (31 %), H→L+2 (69 %)
S_{17}	277	0.0005	H-3→L+1 (94 %)
S_{18}	274	0.0000	H-1→L+3 (78 %), H→L+3 (21 %)
S_{19}	273	0.0271	H-9→L (37 %), H-8→L (27 %), H-7→L (11 %), H-1→L+3 (7 %), H→L+5 (9 %)
S_{20}	271	0.0295	H-3→L+2 (25 %), H-2→L+3 (38 %), H-1→L+6 (7 %), H→L+7(13 %)
S_{21}	271	0.1386	H-3→L+2 (38 %), H-2→L+3 (24 %), H-1→L+6 (12 %), H→L+7(8 %)
S_{22}	269	0.0134	H-10→L (34 %), H-1→L+4 (34 %), H→L+4 (20 %)
S_{23}	267	0.0155	H-10→L (41 %), H→L+4 (48 %)
S_{24}	265	0.0861	H-9→L (42 %), H-8→L (37 %), H-7→L (13 %)
S_{25}	262	0.0050	H-1→L+5 (75 %), H→L+5 (20 %)

S7. Fluorescence spectra of A, D, Al(III)A_3, As–D–A–D, and Sy–D–A–D

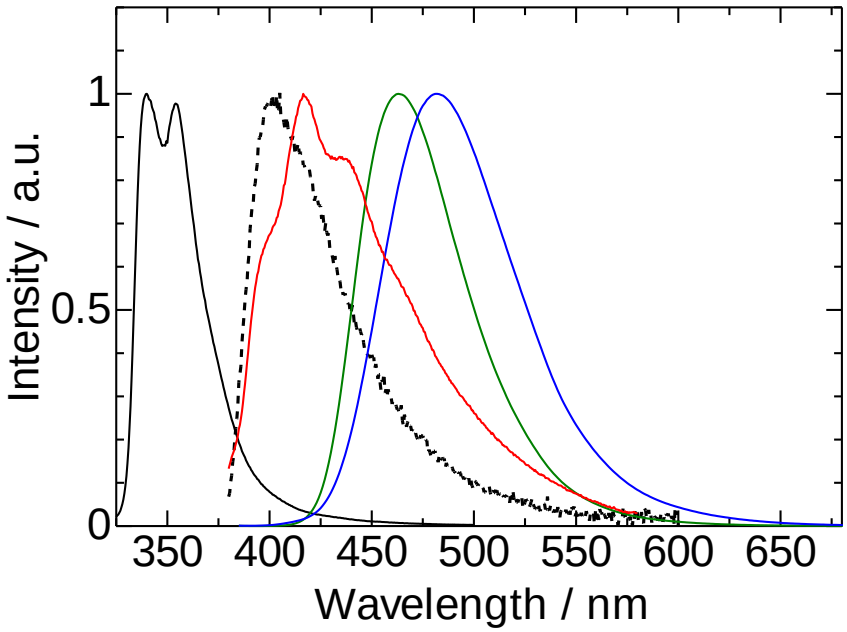

Figure S5. Fluorescence spectra of A (broken line, λ_{ex} = 350 nm), D (black line, λ_{ex} = 295 nm), Al(III)A_3 (red line, λ_{ex} = 350 nm), As–D–A–D (blue line, λ_{ex} = 370 nm), and Sy–D–A–D (green line, λ_{ex} = 370 nm) in $CHCl_3$.

S8. TD-DFT calculation for As–D–A–D in the excited state

In order to clarify the excited state properties, TD-DFT calculations were performed. First, the optimum structure of As–D–A–D in its S_1 state was calculated by the DFT method (B3LYP/6-31G*, Gaussian03). The optimum structure of As–D–A–D showed twisted angles (89.97° and 69.16°) between D and A moieties (Figure 4a). The molecular orbitals and the electronic configurations are shown in Figure S6 and Table S2, respectively.

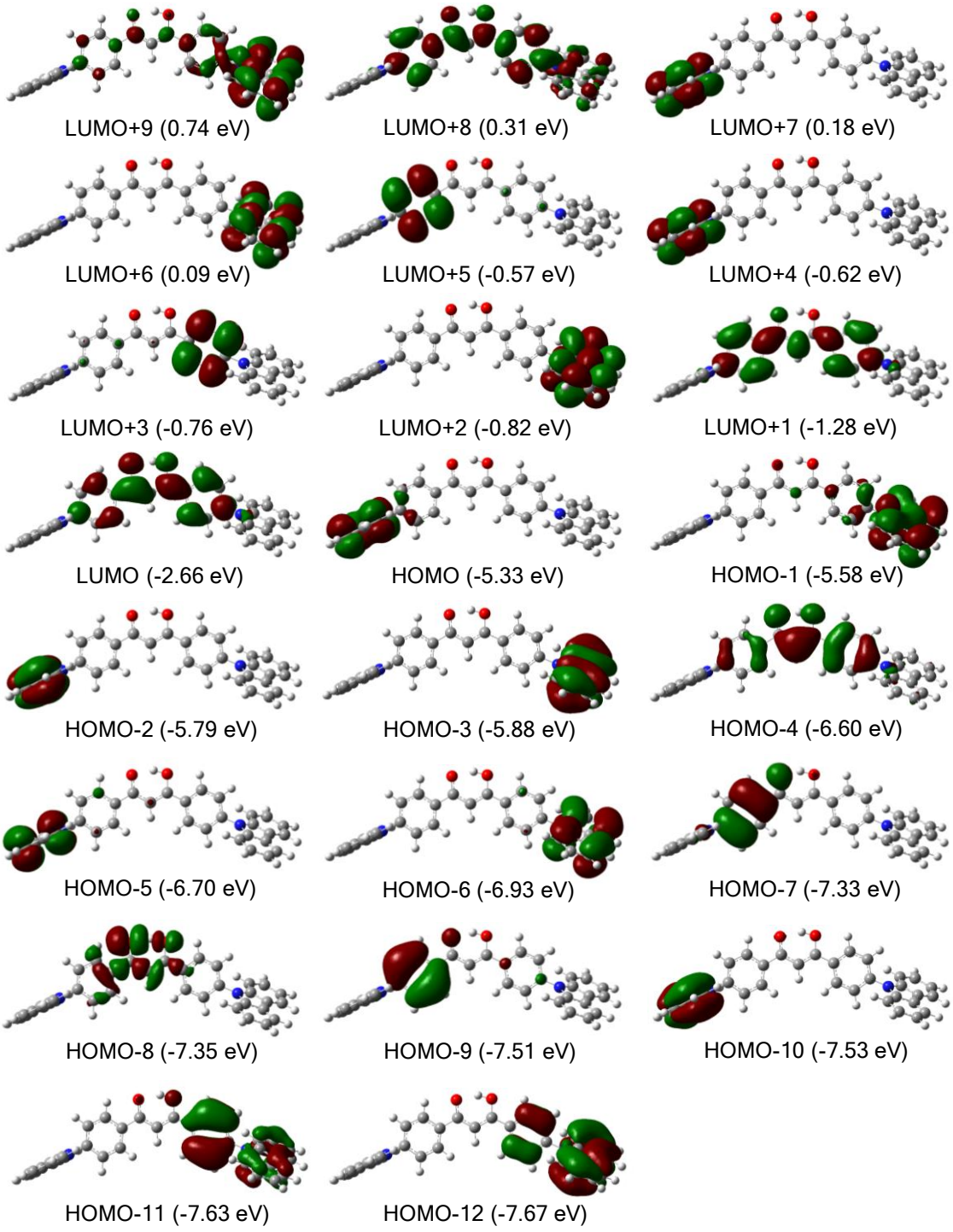

Figure S6. MOs for As–D–A–D in the excited state structure.

Table S2. Information about the main electronic configurations for As–D–A–D.

Excited states	λ_{em} / nm	f_{osc} / -	Main configurations
S_1	548	0.0000	H→L (98 %)
S_2	497	0.1220	H-1→L (99 %)
S_3	446	0.0000	H-2→L (99 %)
S_4	440	0.0000	H-3→L (99 %)
S_5	356	0.0000	H-8→L (97 %)
S_6	351	0.0000	H→L+1 (97 %)
S_7	343	1.0687	H-4→L (96 %)
S_8	337	0.0252	H-5→L (99 %)
S_9	321	0.0019	H-6→L (97 %)
S_{10}	320	0.0025	H-1→L+1 (95 %)
S_{11}	305	0.0268	H-2→L+1 (5 %), H-2→L+7 (6 %), H→L+4 (87%)
S_{12}	304	0.0019	H-2→L+1 (93 %)
S_{13}	303	0.0002	H→L+5 (99 %)
S_{14}	301	0.0249	H-3→L+6 (7 %), H-1→L+2 (89 %)
S_{15}	299	0.0015	H-11→L (5 %), H-1→L+3 (89 %)
S_{16}	295	0.0238	H-9→L (37 %), H-7→L (59 %)
S_{17}	294	0.0002	H-3→L+1 (98 %)
S_{18}	287	0.0000	H→L+2 (15 %), H→L+3 (84 %)
S_{19}	287	0.0000	H→L+2 (85 %), H-8→L (15 %)
S_{20}	282	0.0428	H-12→L (13 %), H-11→L (65 %), H-4→L+3 (6 %), H-1→L+3 (6 %)
S_{21}	282	0.1386	H-9→L (54 %), H-7→L+3 (24 %)
S_{22}	275	0.0000	H-10→L (99 %)
S_{23}	271	0.0117	H-3→L+2 (10 %), H-3→L+3 (86 %)
S_{24}	271	0.0319	H-3→L+4 (60 %), H→L+7 (35 %)
S_{25}	270	0.1018	H-3→L+2 (61 %), H-3→L+3 (11 %), H-1→L+6 (21 %)

S9. TD-DFT calculation for As–D–A–D in the excited state using the other basis set

The optimum structure of As–D–A–D in its S_1 state was calculated using DFT (B3LYP/6-31G**). The optimum structure of As–D–A–D (Figure S7) is similar to the results obtained using the B3LYP/6-31G* basis set. Although it is difficult to determine the exact structure of As–D–A–D, the existence of the undegenerated occupied orbitals (HOMO and HOMO-1) inducing CT hetero-excitons can be confirmed.

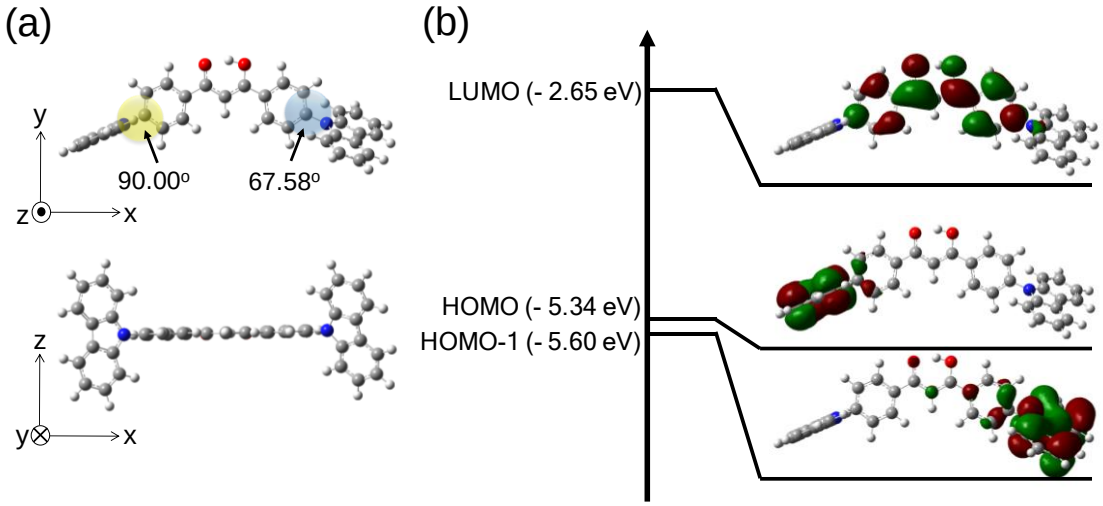

Figure S7. Optimized structure (a) and the molecular orbitals (b, LUMO, HOMO, HOMO-1) for As–D–A–D (B3LYP/6-31G**).

S10. Stokes shifts

Table S3. Stokes shifts estimated by absorption and fluorescence maxima

	Solvent	λ_{abs} / cm^{-1}	λ_{em} / cm^{-1}	Stokes shift / cm^{-1}	Δf
As–D–A–D	Cyclohexane	25,840	23,870	1970	-0.004
As–D–A–D	Hexane	25,970	23,980	1990	0.001
As–D–A–D	Toluene	25,510	22,730	2780	0.014
As–D–A–D	$CHCl_3$	25,580	20,750	4830	0.150
As–D–A–D	CH_2Cl_2	25,640	20,000	5640	0.220
Sy–D–A–D	Toluene	24,940	22,370	2570	0.014
Sy–D–A–D	$CHCl_3$	25,320	21,600	3720	0.150
Sy–D–A–D	CH_2Cl_2	25,250	20,530	4720	0.220

S11. Hydrogenated solvent effect for As–D–A–D

We also consider the presence or absence of the ESIPT pathway from the observed luminescence state for As–D–A–D. The intermolecular interaction between As–D–A–D and halogenated solvents ($CHCl_3$ and CH_2Cl_2) is larger than that between As–D–A–D and other solvents (cyclohexane, hexane, and toluene). The stronger interaction might weaken its intramolecular hydrogen bond, which may decrease the rate constant of ESIPT. Therefore, we checked the photophysical properties of As–D–A–D in CCl_4 with relatively small Δf (= 0.007). The absorption and luminescence spectra of As–D–A–D in CCl_4 are shown in Figure S8. The absorption and luminescence band peaks are 25610 and 23250 cm^{-1}, respectively. The ϕ_f, k_r, and k_{nr} are 4.4 %, 9.6×10^6 s^{-1}, and 2.1×10^8 s^{-1}, respectively. In the solvents, including hydrogenated solvents, the k_{nr} values tend to decrease for As–D–A–D with an increase in Δf. In addition, the k_{nr} values of As–D–A–D and Sy–D–A–D were relatively close. Therefore, these facts suggest that the ESIPT doesn't occur from the observed luminescence states.

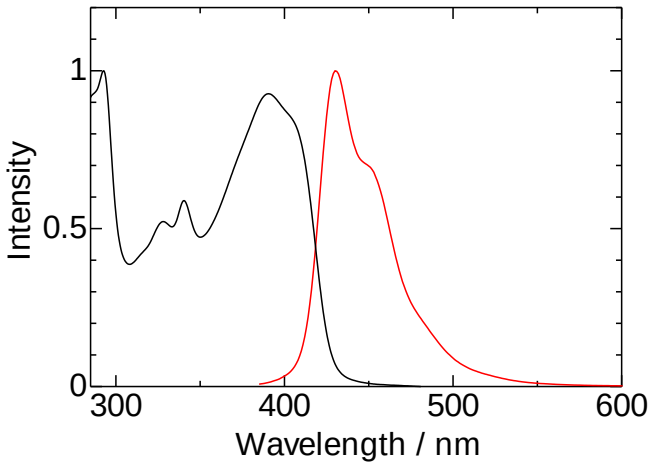

Figure S8. Electronic absorption and luminescence spectra of As–D–A–D in CCl_4. Normalized by intensity maxima.

S12. Conceptual diagram of the change of the twisted angles with increase in Δf

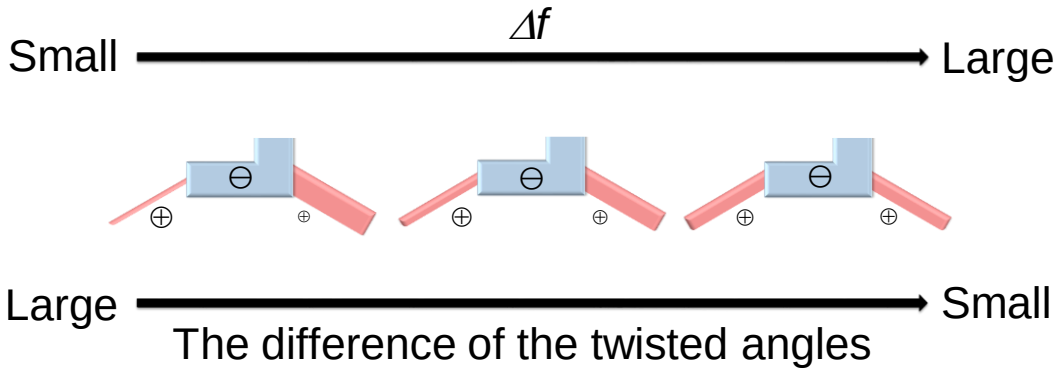

Figure S9. Conceptual diagram of the change of the twisted angles with increase in Δf.

S13. Organic compound with an inversion energy level between S_1 and T_1

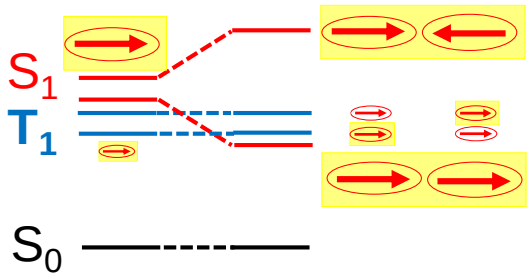

Figure S10. Organic compound with an inversion energy level between S_1 and T_1.